CrystEngComm

Hollow copper-ceria microspheres with single and multiple shells for preferential CO oxidation

SCHOLARONE™
Manuscripts

Journal Name

ARTICLE

Hollow copper-ceria microspheres with single and multiple shells for preferential CO oxidation

Xie Yu, [‡][a] Jingfang Wu, [‡][a] Aiai zhang,[a] Lei Xue,[a] Qi Wang,[a] Xiaopeng Tian,[a] Shiyao Shan,[b] Chuan-Jian Zhong[b] and Shanghong Zeng*[,a]

The architecture of catalyst particles plays an important role in determining the catalytic properties. However, the challenge is the ability to tune the architecture at nanoscale. Herein we report the design and construction of hollow CuO/CeO_2 microspheres with controllable shells, which exhibit significantly enhanced catalytic performance. The hollow CuO/CeO_2 microspheres with single and multiple shells were synthesized by self-templating method. The catalytic activity of the catalysts for preferential CO oxidation is shown to increase with increasing the number of the spherical shells. A maximized performance is observed for the triple-shelled catalyst, reaching CO conversion of 100% and CO_2 selectivity of 91% at 95 °C. The triple-shelled catalyst also displays a broad temperature window for CO total conversion from 95 °C to 195 °C. The findings are attributed to the enhanced exposure of the active sites on the surface of the triple-shelled architecture, fine-tunable geometric and electronic interaction, and increased space inside the catalyst, which together amplify the reactant access and interaction.

1. Introduction

The high demand for sustainable energy and clean environment has triggered intensive interests in proton exchange membrane fuel cells (PEMFCs) [1] Hydrogen, as fuel of PEMFCs, is generated by auto-thermal reforming of hydrocarbons in combination with water-gas shift reaction, leading to the presence of a small amount of CO in H_2-rich gasses, which could poison Pt anode of PEMFCs. Three methods including Pd-membrane separation, catalytic methanation and preferential CO oxidation have been developed to remove CO to a trace level (below 10 ppm) from H_2-rich gasses. Among them, preferential CO oxidation (CO-PROX) is regarded as an effective way to eliminate CO and minimize the loss of hydrogen.[2,3] The development of catalysts over CO-PROX has been focused on ceria-based composites, including cerium-zirconium solid solution in three-way catalytic converters. In 1995, Liu and Flytzani-Stephanopoulos reported the composition and activity of transition metal-fluorite catalysts for CO and CH_4 oxidation.[4] The CuO/CeO_2 catalysts were found to have promising catalytic performance by comparing with noble metal catalysts in consideration of earth abundance and low cost. The superior catalytic performance of CuO/CeO_2 catalysts was due to the synergistic redox properties via Ce^{4+}/Ce^{3+} and Cu^{2+}/Cu^+ redox cycles as well as interfacial interaction between copper and ceria.[5] Changing the geometrical shapes of catalysts could tune the geometric interaction, which is closely associated with catalytic performance.[6-8] Although numerous studies have focused on preparing CeO_2 with controllable shapes containing different crystal planes to further improve the activity and selectivity for CO-PROX, the ability to control the interior architectures of the CuO/CeO_2 catalysts remains challenging. [9-12] Recently, Li et al. developed a kind of litchi-peer-like hollow CuO/CeO_2 microspheres for CO oxidation. And they found that the litchi-peel-like sample with 20% Cu demonstrated the outstanding catalytic activity and stability due to step-stabilized strong interaction between CuO and CeO_2.[13] Moreover, the multilevel-structured micro/nanomaterials with increased active surfaces have attracted considerable interests in potential applications such as drug delivery, energy systems and nanocatalysis.[14-17] However, little is currently known about how to design and construct such hollow or multilevel architectures at atomic level to improve the catalytic performance for CO-PROX. The effect of how the shell numbers of the multi-shell catalysts on the catalytic activity is basically unknown.

In this report, we show the ability to engineer the CuO/CeO_2 multilevel structures towards promoting the catalytic performances for CO-PROX reaction. To the best of our knowledge, there has been no report demonstrating the ability to form multilevel-structured CuO/CeO_2 catalysts. We will show a self-templating method to synthesize the hollow CuO/CeO_2 microspheres with tunable single, double and triple

[a.] Inner Mongolia Key Laboratory of Chemistry and Physics of Rare Earth Materials, School of Chemistry and Chemical Engineering, Inner Mongolia University, Hohhot 010021, China. Emails: zengshanghong@imu.edu.cn
[b.] Department of Chemistry, State University of New York at Binghamton, Binghamton, New York 13902, United States. Emails: cjzhong@binghamton.edu
† Electronic Supplementary Information (ESI) available: Experimental details and figures. See DOI: 10.1039/x0xx00000x
‡ These authors contributed equally to this work.

shells, aiming at establishing the correlation between catalytic activities and the number of shells.

2. Experimental Section

2.1. Chemicals

All of the chemicals in our experiments were analytical grade and used without further purification. Cerium chloride hydrate (99.0%), Cerium nitrate hexahydrate (99.0%) and copper nitrate (99.0%) were purchased from Tianjin FengChuan Chemical Research Institute (Tianjin, China). Ethanol (99.7%), PEG600, glucose, PVP and ethylene glycol were purchased from Tianjin Guangfu Fine Chemical Research Institute (Tianjin, China).

2.2. Catalyst Preparation

The self-templating method was performed to prepare the CeO_2 hollow spheres with multi-shelled interior structures. The synthetic process involves dissolution of Ce precursors in aqueous solution by hydrothermal and calcination treatments, and more details are as follows.

Single-shelled CeO_2 hollow microspheres (SSCeO$_2$). 2g $Ce(NO_3)_3 \cdot 6H_2O$ and 0.8 g PVP were dissolved in mixed solution including 56 mL ethylene glycol and 8 mL soft water, and stirred for 30 min. Then the above solution was transferred into 80 mL Teflon-lined stainless-steel autoclave and heated at 160 °C for 8 h. The suspension was washed by distilled water and ethyl alcohol, then dried at 60 °C for 12 h. Finally, the sample was calcined at 400 °C for 2 h in air.

Double-shelled CeO_2 hollow microspheres (DSCeO$_2$). The DSCeO$_2$ were prepared according to the reported literature with a little modification.[18] 1.5 g $Ce(NO_3)_3 \cdot 6H_2O$ was dissolved in mixed solution including 45 mL PEG600 and 15 mL deionized water by stirring for 1 h. Then the above solution was transferred into 80 mL Teflon-lined stainless-steel autoclave and heated at 180 °C for 24 h. The white precipitate was collected by centrifuging several times with distilled water and ethyl alcohol, then dried in air at 80 °C for 5 h. Finally, the sample was calcined at 400 °C for 2 h in air to remove the organic template.

Triple-shelled CeO_2 hollow microspheres (TSCeO$_2$). 1.128 g urea was dissolved in 36 mL deionized water, and then 0.402 g $CeCl_3 \cdot 7H_2O$ was added and stirred for 15 min. The 120 mL glucose (10.8 g) aqueous solution was added in above solution and vigorous stirred until forming a clear solution. Subsequently, the solution was transferred to the Teflon-lined stainless-steel autoclave and heated at 160 °C for 20 h. After cooling to room temperature naturally, the suspension was washed by distilled water and ethylalcohol, then dried at 100 °C in air for 12 h. Finally, the sample was calcined at 400 °C for 1 h in air. The light-yellow powder was obtained.

Multi-shelled CuO/CeO_2 hollow-microsphere catalysts (MSCuO/CeO$_2$). MSCuO/CeO$_2$ catalysts were prepared by incipient wetness impregnation method by using $Cu(NO_3)_2 \cdot 3H_2O$ solution. The molar ratio of Cu/Ce was 1/4 in every sample. After impregnation, the samples were dried at 80 °C for 24 h and calcined at 300 °C for 2 h in air. The catalysts were named as SSCuO/CeO$_2$ (single-shelled CuO/CeO$_2$ hollow microsphere), DSCuO/CeO$_2$ (double-shelled CuO/CeO$_2$ hollow microsphere) and TSCuO/CeO$_2$ (triple-shelled CuO/CeO$_2$ hollow microsphere).

2.3. Catalyst Characterizations

Transmission electron microscopy (TEM) images were taken on a Tecnai G2 F20 S-Twin instrument with an acceleration voltage of 200 kV. The samples were dispersed in ethanol with the ultrasonic treatment. Powder X-ray diffraction (XRD) patterns were recorded on a PANalytical X'pert PRO diffractometer with Cu Kα source (λ=0.1542 nm) in the range of 2θ between 20° and 80°. The average crystallite sizes were estimated from the Scherrer's equation. N_2 adsorption-desorption isotherms were obtained at liquid nitrogen temperature (-196 °C) on a Micrometrics ASAP2020 adsorption apparatus. The samples were degassed under a vacuum of 10^{-5} Torr for 12 h at 200 °C. The surface area and pore size distribution were determined by the Brunauer-Emmett-Teller (BET) and the Barrette-Joynere-Halenda (BJH) methods, respectively. X-ray photoelectron spectroscopy (XPS) analyses were performed on a Thermo ESCALAB 250XI with monochromatic Al Kα radiation (150 W, 1486.6 eV), where the spectra of samples were recorded with the constant pass energy value of 25 eV and the X-ray spot of 500 μm. H_2 temperature-programmed reduction (H$_2$-TPR) was conducted on a Micromeritics Apparatus (AutoChem Ⅱ 2920). The reduction gas was 10 % H_2/Ar mixture, and the flow rate was 50 mL/min. Before reduction, the 100 mg of samples was placed on the top of silica wool in a quartz reactor, and pretreated at 200 °C for 1 h in N_2 stream in order to remove the contaminants. Then the H_2/Ar mixture was switched on, and the sample was heated with a heating rate of 10 °C/min. The reaction was performed from room temperature to 900 °C.

2.4. Catalytic Performance Tests

Catalytic performance tests were carried out on a tubular quartz microreactor. The reaction mixture consisted of 1.0 vol% CO, 1.0 vol% O_2 and 50.0 vol% H_2 with N_2 as balance gas. The catalysts were grinded and sieved by 200-mesh sieve in order to ensure the elimination of internal diffusion, and then the catalysts were mixed with quartz sand. The space velocity was 40,000 mL/($g_{cat} \cdot$h), and the temperature was from 35 to 215 °C. The inlet and outlet streams were measured by using an online GC-2014C gas chromatograph equipped with a thermal conductivity detector (TCD). The CO, O_2 and N_2 were separated by a 5A molecular sieve column, and CO_2 was separated by a TDX column. The CO conversion and CO_2 selectivity were calculated according to the following equations (1) and (2).[19]

$$\text{CO coversion (\%)} = \frac{[CO]_{in} - [CO]_{out}}{[CO]_{in}} \times 100\% \tag{1}$$

$$\text{CO}_2 \text{ selectivity (\%)} = \frac{0.5([CO]_{in} - [CO]_{out})}{[O_2]_{in} - [O_2]_{out}} \times 100\% \tag{2}$$

where in and out were inlet and outlet concentrations of CO and O_2.

3. Results and discussion

3.1. Morphologies and structures

The morphologies and structures of the three as-synthesized CuO/CeO_2 hollow microspheres with multi-shells are revealed by several characterizations (Fig. 1, Fig. 2 and Fig. S1). It is noted that the CeO_2 supports still keep the multi-shelled hollow microspheres after supporting CuO particles. The crystallite sizes of CeO_2 increase and then decrease with increasing the shells in the range of 0.1-1.0 µm. Instead, the crystallite sizes of CuO gradually decrease as increasing the number of shells (Table 1). The improved dispersion of copper species could be due to the enhanced the interaction between copper and ceria by increasing the number of ceria layers. The transmission electron microscopy (TEM) clearly shows that the $TSCuO/CeO_2$ structure is generated as the form of hollow sphere morphology with three shells (Fig. 1a). The shells are enriched with the elements of Ce, Cu and O detected by scanning transmission electron microscopy (STEM) and elemental mapping (Fig. 1b), which are in agreement with the result from the corresponding line-scan profiles (Fig. 1d). Specifically, the shells consist of the CeO_2 nanoparticles with high crystallinity, and the lattice spacing is mainly 0.31 nm corresponding to CeO_2 (111) plane. The CuO particles are dispersed on the surface of CeO_2 shells, and lattice spacing of 0.25 nm corresponds to CuO (002) plane (Fig. 1c). Meanwhile, the powder X-ray diffraction (XRD) patterns display the characteristic peaks of fluorite-type CeO_2 (PDF#98-005-4356) and two weak peaks of CuO at 35.6 and 38.7° (PDF#98-005-9563), also confirming that the $SSCuO/CeO_2$, $DSCuO/CeO_2$, and $TSCuO/CeO_2$ catalysts are composed of the CuO and CeO_2 (Fig. 1f and Fig. S2).

In addition, as shown in Table 1, the lattice parameters of CeO_2 in all the multi-shelled CuO/CeO_2 hollow microspheres are smaller than their corresponding CeO_2 supports, because some Cu^{x+} species with smaller ionic radius got into ceria lattice and partially replaced Ce^{4+} to form solid solution. The formation of oxygen vacancies on the CeO_2 surface could facilitate the incorporation of Cu^{x+} into ceria lattice, as well as generate the chemical interaction between copper and ceria. Especially, there are the smallest lattice parameter of CeO_2

and crystallite sizes of CeO_2 and CuO in the $TSCuO/CeO_2$ catalyst, demonstrating that the CeO_2 support had strong contact and interaction with CuO. This would lead to producing superior synergistic effect in the CuO/CeO_2 binary system.
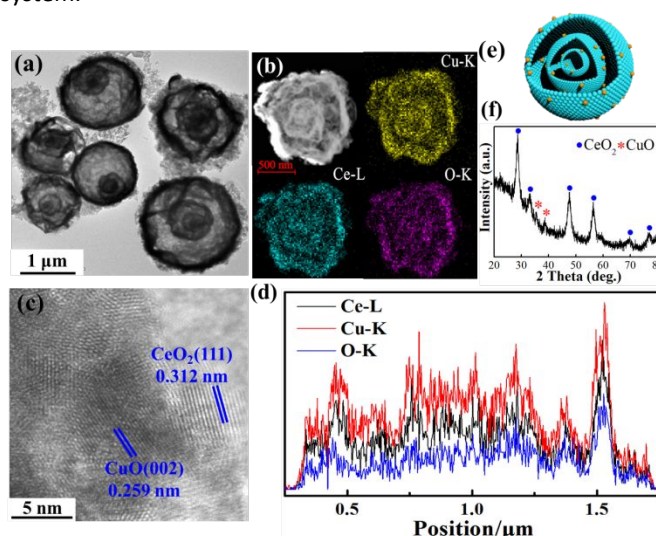

Fig. 1 (a and c) TEM images, (b) STEM and element mapping images, (e) the corresponding model of (a), (d) the corresponding line-scan profiles and (f) XRD pattern of the $TSCuO/CeO_2$ catalyst.
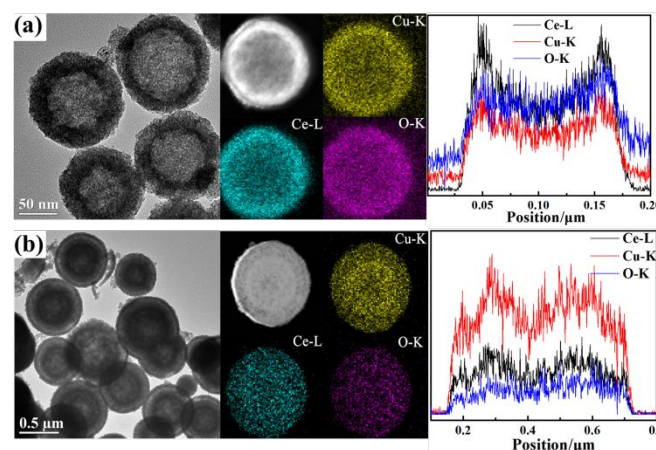

Fig. 2 TEM, STEM, element mapping images and corresponding line-scan profiles for (a) $SSCuO/CeO_2$ and (b) $DSCuO/CeO_2$ catalysts.

Table 1 Structure and textural properties of the supports and catalysts

Sample	CeO$_2$ Lattice parameter (Å)	Particle size (nm)		Pore volume (cm^{3}g^{-1})	Pore size (nm)
		d(CuO)[a]	d(CeO$_2$)[b]		
SSCeO$_2$	5.417	- -	8.0	0.10	3.83
SSCuO/CeO$_2$	5.405	38.8	6.8	0.10	3.82
DSCeO$_2$	5.411	- -	13.9	0.11	3.80
DSCuO/CeO$_2$	5.408	37.6	13.4	0.09	3.82
TSCeO$_2$	5.412	- -	6.5	0.20	3.81
TSCuO/CeO$_2$	5.401	20.0	5.3	0.11	3.82

[a] Calculated from the Scherrer equation according to the (002) diffraction peaks of CuO. [b] Calculated from the Scherrer equation according to the (111) diffraction peaks of CeO_2.

Meanwhile, the porous properties of the catalysts were characterized by the N₂ adsorption/desorption technique. As shown in Fig. S3, all the samples present IV-type adsorption-desorption isotherms with a H3-type hysteresis loop, indicating the existence of a mesoporous structures.[20] It can be seen from Table 2 that the TSCuO/CeO₂ catalyst owns the largest BET surface area (86 m²g⁻¹) among all the multi-shelled CuO/CeO₂ hollow microspheres. It indicates that TSCuO/CeO₂ facilitates the distribution of the active species; hence the CuO nanoparticles have the smallest crystallite size in the TSCuO/CeO₂ catalyst.

3.2. Surface properties

Subsequently, X-ray photoelectron spectroscopy (XPS) was used to detect the surface properties of the multi-shelled CuO/CeO₂ hollow microspheres. The Cu 2p, Ce 3d and O 1s core-level spectra are shown in Fig. 3. Obviously, Cu^{2+} species from CuO are present in all the catalysts, which is substantiated by the main peak of Cu 2$p_{3/2}$ at 934.6 eV with the shake-up satellite peak around 939.0-946.0 eV.[21, 22] The position of the Cu 2$p_{3/2}$ peak at 933.2 eV indicates the existence of reduced Cu species (mainly Cu$^+$, and see Fig. S4). The presence of Cu$^+$ species results from the synergistic effect between copper and ceria, and the Cu$^+$ species are proposed as the CO adsorption sites for CO-PROX.[23] The reduction degree of Cu^{2+} can be estimated by the ratio of the intensities of shake-up satellite peaks to those of the main peaks (I_{sp}/I_{mp}).[24] As shown in Table 2, all the catalysts exhibit lower I_{sat}/I_{main} values than 0.57 for pure CuO, further suggesting the presence of Cu$^+$ species. Interestingly, the reduction degree of Cu^{2+} increases as increasing the shells of microsphere, which is closely associated with the defects and imperfections of ceria. The existence of defects and imperfections could generate strong interaction between copper and ceria. Furthermore, the TSCuO/CeO₂ has the lowest value of I_{sp}/I_{mp}, indicating a maximum amount of the reduced Cu species, which is closely associated with the dispersion of CuO nanoparticles and synergistic interaction between CuO and CeO₂ on the triple-shelled structure.
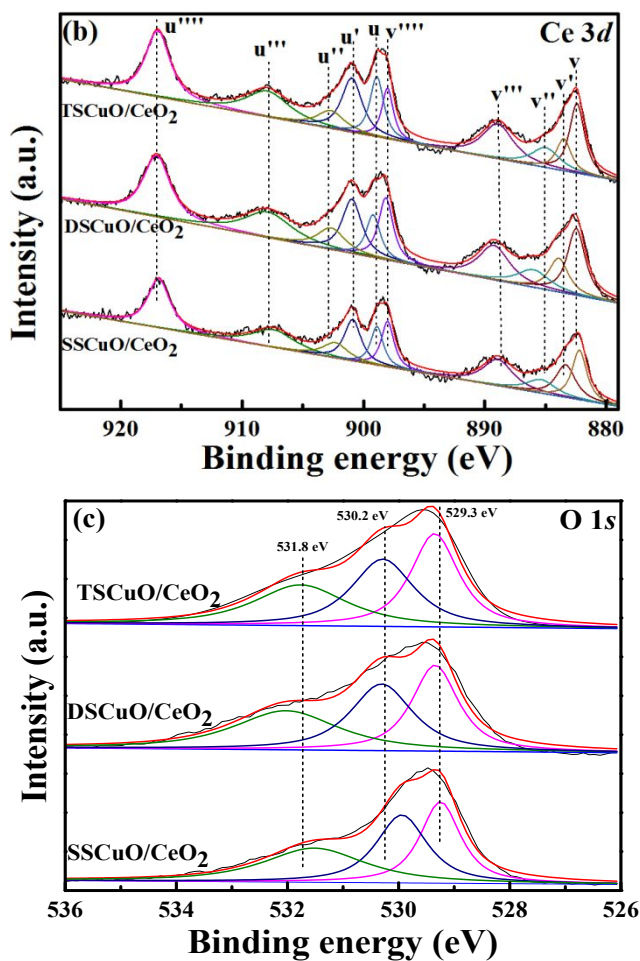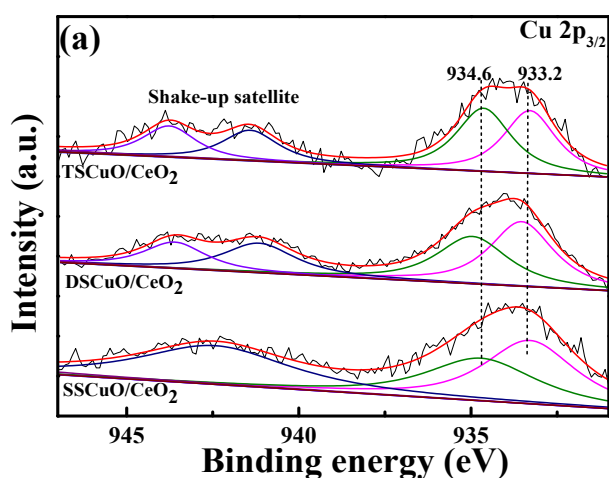

Fig. 3 XPS spectra of (a) Cu 2p, (b) Ce 3d and (c) O 1s regions for the hollow microspheres.

The Ce 3d spectra are composed of two sets of spin-orbital multiples, which are related to 3$d_{3/2}$ and 3$d_{5/2}$, labelled as u-u'''' and v-v'''', respectively (Fig. 3b). Among the ten peaks, u, v, u'' and v'' were assigned to Ce^{3+}, whereas the others belonged to Ce^{4+} species. Generally, the surface Ce^{3+} is accompanied by the presence of oxygen vacancies, which are beneficial to transfer electrons during CO adsorption.[25] The content of surface Ce^{3+} can be obtained by considering the relative area of Ce^{3+} peaks and the total Ce 3d peaks denoted as Ce^{3+} (%).[26] And the concentration of oxygen vacancies, namely [V$_O$], can be calculated by [V$_O$] = 1- (3[Ce^{3+}] + 4[Ce^{4+}])/4 .[27] As shown in Table 2 and Fig. S5, the content of Ce^{3+} and oxygen vacancies increase with supporting CuO as well as increasing the shells of microsphere. This can be attributed to the selective binding of adsorbed Cu atoms at stoichiometric sites on the CeO₂ (111) surfaces and the electronic interaction between copper and ceria.[28] The increase of shells increases the contact interface and enhances the electronic interaction of metal-support, resulting in the increase of Ce^{3+} concentration. Herein, the electronic interaction can generate new active sites on the interface due to the modification of oxide surface. The TSCuO/CeO₂ catalyst exhibits the highest content of Ce^{3+} and oxygen vacancies compared to the SSCuO/CeO₂ and DSCuO/CeO₂ catalysts. The Ce^{3+}, which is capable of reducing

copper oxides, may shift the redox equilibrium of $Cu^{2+} + Ce^{3+} \rightarrow Cu^{1+} + Ce^{4+}$ from left to right, thus the active Cu^+ species for CO-PROX reaction generate at the interface.

Moreover, the overlapped peaks of O $1s$ spectra are decomposed into three peaks at about 529.3 eV, 530.2 eV and 531.8 eV (Fig. 3c), assigned to the lattice oxygen, the surface chemisorbed oxygen, and oxide defects or -OH groups, respectively.[29, 30] From XPS analysis, it reveals that the electronic interaction between copper and ceria conduces to the co-existence of Cu^{2+}/Cu^+ and Ce^{4+}/Ce^{3+} redox pairs as well as defect oxygen on the surface of the multi-shelled CuO/CeO_2 hollow microspheres.

Table 2 BET surface area and XPS results of the catalysts

Catalyst	S_{BET} (m^2g^{-1})	XPS data		
		Ce^{3+} (%)	I_{sp}/I_{mp}	$[V_O]$ (%)
SSCuO/CeO$_2$	33	22.6	0.55	5.65
DSCuO/CeO$_2$	39	24.3	0.50	6.08
TSCuO/CeO$_2$	86	25.8	0.49	6.45

3.3. Redox properties

The H_2 temperature programmed reduction (H_2-TPR) was applied to obtain the redox properties of the samples. Konsolakis and Ioakeimidis reported that owing to surface oxygen reduction the H_2 amount for the reduction of CuO/CeO_2 catalysts surpasses that for the complete reduction of copper oxides.[31] As shown in Fig. 4, there are two reduction peaks at lower temperature for the TSCuO/CeO$_2$ catalyst, corresponding to well-dispersed Cu species (α) and medium-sized CuO (β).[27] However, only β peak can be observed in the profiles of SSCuO/CeO$_2$ and DSCuO/CeO$_2$. For TSCuO/CeO$_2$ catalyst, the reduction peak (γ) at 450 °C was attributed to the

reduction of surface Ce species. The reduction peaks (δ) at about 750 °C correspond to the reduction of bulk CeO_2. It is evident that the reduction temperature of bulk CeO_2 shifts to lower temperature with increasing the number of shells from single to triple, indicating the increase of the defects and imperfections on ceria. As a result, the triple-shelled CuO/CeO_2 hollow microsphere has the lowest reduction temperature of bulk CeO_2. In addition, there is an obvious reduction peak of surface ceria above-mentioned in the profile of the triple-shelled CuO/CeO_2 catalyst. These alterations of the reduction temperature of ceria strongly depend on the work function of copper species, confirming the electronic nature of copper-ceria interaction.[32]
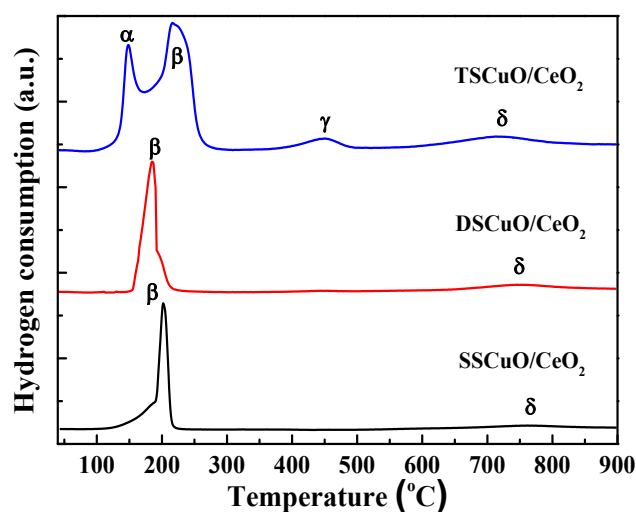

Fig. 4 H_2-TPR profiles of the multi-shelled CuO/CeO_2 hollow microspheres.

Table 3 Comparison of catalytic performance in CO-PROX over multi-shelled CuO/CeO_2 hollow microspheres and reported copper-cerium oxide catalysts

Catalysts	Operating conditions	GHSV	T_{50}^a (°C)	T_{100}^b (°C)	CO_2-selectivity at T_{100} (%)	Width^c	Ref.
TSCuO/CeO$_2$	1% CO, 1% O$_2$, 50% H$_2$ in N$_2$	40,000 (mL·g_{cat}^{-1}·h^{-1})	67	95	91	100	This work
DSCuO/CeO$_2$	1% CO, 1% O$_2$, 50% H$_2$ in N$_2$	40,000 (mL·g_{cat}^{-1}·h^{-1})	80	135	65	60	This work
SSCuO/CeO$_2$	1% CO, 1% O$_2$, 50% H$_2$ in N$_2$	40,000 (mL·g_{cat}^{-1}·h^{-1})	105	155	66	40	This work
CuCe bulk	1% CO, 1% O$_2$, 50% H$_2$ in N$_2$	40,000 (mL·g_{cat}^{-1}·h^{-1})	--	160	66	30	33
6CuCe	1.25% CO, 1.25% O$_2$, 50% H$_2$ in He	22,000 (h^{-1})	95	140	63	25	34
CuCe	1% CO, 1% O$_2$, 60% H$_2$ in He	12,000 (h^{-1})	95	155	40	45	35
CuCe(rod)	1% CO, 1% O$_2$, 50% H$_2$ in Ar	60,000 (mL·g_{cat}^{-1}·h^{-1})	67	100	100	40	36
10CuCe	0.5% CO, 0.9% O$_2$, 50% H$_2$ in N$_2$	66,000 (mL·g_{cat}^{-1}·h^{-1})	90	115	100	30	37

Reaction conditions: 1 vol% CO, 1 vol% O$_2$, 50 vol% H$_2$ and N$_2$ balance; GHSV = 40000 mL·g^{-1}·h^{-1}; Temperature range = 35- 215 °C; atmospheric pressure.
^{a}T_{50}: Temperature at 50% CO conversion; ^{b} T_{100}: Temperature at 100% CO conversion; ^{c} Width: Width of temperature window (CO conversion > 99.0%).

3.4. Catalytic activities for CO-PROX

The performance tests were carried out by using the synthetic gasses (1 vol% CO, 1 vol% O_2, 50 vol% H_2 and N_2 balance) and the space velocity of 40000 $mL \cdot g^{-1} \cdot h^{-1}$ in the temperature range of 35-215 ^oC. As shown in Table 3, the triple-shelled CuO/CeO_2 hollow microspheres display wider temperature window of total CO conversion in contrast to the $SSCuO/CeO_2$ and $DSCuO/CeO_2$ catalysts. At the same time, the $TSCuO/CeO_2$ has the lowest temperatures for 50% and 100% CO conversion, denoted as T_{50} and T_{100}, respectively. Even more remarkably, the $TSCuO/CeO_2$ catalyst also exhibits better or similar catalytic performance compared to the copper-cerium oxide catalysts with solid structures reported in the literatures in Table 3.[33-37] The catalytic activities are in the order of $TSCuO/CeO_2$ > $DSCuO/CeO_2$ > $SSCuO/CeO_2$, and it is interesting that the catalytic activity increases with increasing the number of shells. It is the first time to build a correlation between the catalytic activities with the number of shells for CO-PROX. The catalyst with unique triple-shelled structure possesses largest surface area for the dispersion of active sites, hence resulting in improved catalytic activity. Moreover, the small crystallite sizes of CeO_2 and CuO in the $TSCuO/CeO_2$ catalyst promote its synergistic redox properties. Furthermore, the surface Ce species and CuO interact to generate large amount of Cu^+ and Ce^{3+}, as displayed in XPS analysis, which facilitate the formation of oxygen vacancies and enhance the synergistic interaction of Cu-Ce species. As shown in Fig. 5a, CO_2 selectivity of all the samples drops when the reaction temperature reaches 95 ^oC, because of the competitive oxidation reaction of H_2 and O_2. Despite this, the catalysts can still keep 100% CO conversion up to 195 ^oC. Combined with the analyses of products in Fig. 5b, the $TSCuO/CeO_2$ catalyst keeps the highest CO_2 selectivity at the temperature of T_{50} and T_{100}, respectively. As a result, the $TSCuO/CeO_2$ catalyst achieves a relatively optimum performance based on CO conversion and CO_2 selectivity.

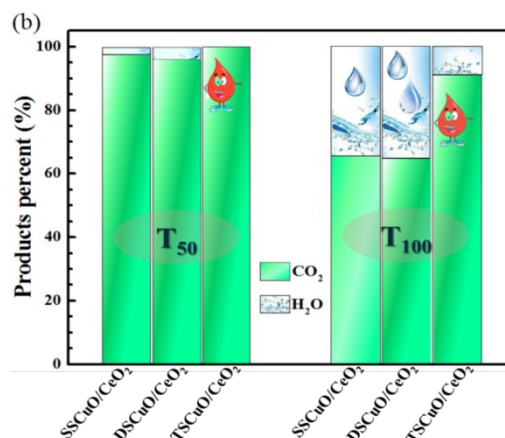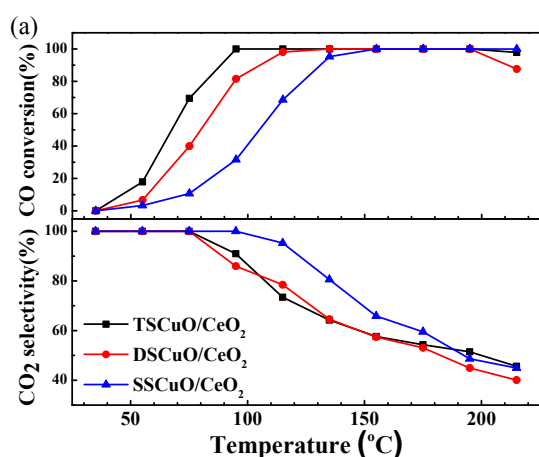**Fig. 5** (a) CO conversion and CO_2 selectivity over the catalysts; (b) product percent of O_2 conversion at the temperature of T_{50} and T_{100} for 50% and 100% CO conversion, respectively.

3.5. Mechanistic considerations of the catalytic synergy

The above results provide not only an insight into some of the previous studies on the mechanism for CO-PROX over copper-cerium oxide catalysts, but also a new strategy to tune the catalytic synergy. We believe that CO in rich-H_2 streams absorbs on the reduced Cu^+ species at the contact interface of copper and cerium species, and then reacts with lattice oxygen to form CO_2.[38,39] The formation of reduced Cu^+ species follows a redox reaction path involving $Cu^{2+} + Ce^{3+} \rightarrow Cu^{1+} + Ce^{4+}$. And the Cu^+ species are stabilized through the interaction with ceria.[40] In the process of CO-PROX, the formation of reduced Cu^+ species, Ce^{3+} species and surface oxygen vacancies could jointly promote the synergistic effect between copper and cerium towards enhancing catalytic performance. Herein the excellent catalytic performance of the $TSCuO/CeO_2$ catalyst for CO-PROX is attributed to the large surface area and the surface-enhanced dispersion of active sites, which are further confirmed by the change of Cu dispersion and TOF values in Table S3. As illustrated in Fig. 6, the hollow spheres with more shells are able to provide an increased space for the reactant access and interaction inside the catalyst. Thus it facilitates the CO oxidation at the contact interface of copper and cerium species. Meanwhile, the triple-shelled structure is favorable for the formation of surface Ce species via increasing the defects and imperfections on ceria. And the surface Ce species could lead to the formation of large amount of Cu^+ through promoting the reaction of $Cu^{2+} + Ce^{3+} \rightarrow Cu^{1+} + Ce^{4+}$. The oxygen vacancies with a high concentration also improve the reduction of copper species and enhance the synergistic interaction of Cu-Ce species. Therefore, the triple-shelled CuO/CeO_2 hollow microsphere catalyst shows a greatly enhanced catalytic performance for preferential CO oxidation.
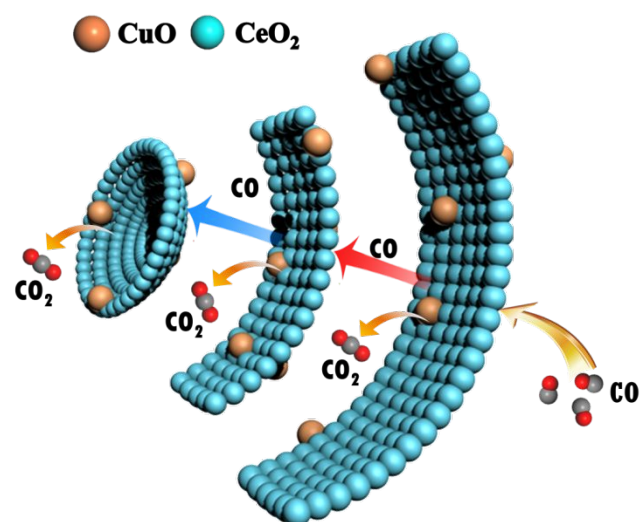
ARTICLE

Fig. 6 Schematic diagrams for CO-PROX over the CuO/CeO$_2$ hollow microspheres catalysts with triple shells.

4. Conclusions

In conclusion, we have demonstrated a new strategy for enhancing the catalytic performance for CO-PROX by tuning the number of shells over the copper-cerium oxide catalysts. The multi-shelled CuO/CeO$_2$ hollow microspheres were constructed by the self-templating method combined with hydrothermal and calcination treatments. The TSCuO/CeO$_2$ catalyst exhibits 100% CO conversion at temperature window of 95 ^{o}C to 195 ^{o}C. Its outstanding catalytic performance is attributed to the unique catalytic synergy of the triple-shelled structure. That is, the triple-shelled hollow structure not only enhances the geometric and electronic interaction between copper and ceria, but also increases the distribution of reduced Cu$^+$ and Ce^{3+} species on the surface. This catalytic synergy leads to the enhanced exposure of the active sites on the catalyst surface and the increased space inside the catalyst to amplify reactant access and interaction. The understanding of the morphology and structure in this work may also offer a new strategy for the design of highly efficient catalysts for many other catalytic reactions.

Conflicts of interest

There are no conflicts to declare.

Acknowledgements

Notes and references

1   L. L. Zhang, S. Q. Zhu, Q. W. Chang, D. Su, J. Yue, Z. Du and M. H. Shao, *ACS Catal.*, 2016, **6**, 3428.
2   T. Baidya, T. Murayama, P. Bera, O. Safonova, P. Steiger, N. Katiyar, K. Biswas and M. Haruta, *J. Phys. Chem. C,* 2017*,* **121,** 15256.
3   J. F. Ding, L. P. Li, H. X. Li, S. Q. Chen, S. F. Fang, T. Feng, and G. S. Li, *ACS Appl. Mater. Interfaces,* 2018, **10**, 7935.
4   W Liu and M Flytzanistephanopoulos, *J. Catal.,* 1995, **153**, 304.
5   J. W. Qin, J. F. Lu, M. H. Cao and C. W. Hu, *Nanoscale*, 2010, **2**, 2739.
6   W. X. Huang and Y. X. Gao, *Catal. Sci. Technol.,* 2014, **4**, 3772.
7   S. Y. Chen, E. Tseng, Y. T. Lai, W. Lee and A. Gloter, *Nanoscale*, 2017, **9**, 10764.
8   P. Strasser, M. Gliech, S. Kuehl and T. Moeller, *Chem. Soc. Rev.*, 2018, **47**, 715.
9   A. Trovarelli and J. Llorca, *ACS Catal.*, 2017, **7**, 4716.
10 X. L. Guo, J. X. Mao and R. X. Zhou, *J. Power sources*, 2017, **371**, 119.
11 S. Y. Song, X. C. Liu, J. Q. Li, J. Pan, F. Wang, Y. Xing, X. Wang, X. G. Liu and H. J. Zhang, *Adv. Mater.*, 2017, **29**, 1700495.
12 Y. Zhao and L. Jiang, *Adv. Mater.*, 2009, **21**, 3621.
13 W. G. Li, Y. J. Hu, H. Jiang, N. Jiang, W. Bi and C. Z. Li, *Nanoscale*, 2018, **10**, 22775.
14 J. Qi, K. Zhao, G. D. Li, Y. Gao, H. J. Zhao, R. B. Yu and Z. Y. Tang, *Nanoscale*, 2014, **6**, 4072.
15 H. Ren, R. B. Yu, J. Y. Wang, Q. Jin, M. Yang, D, Mao, D, Kisailus, H. J. Zhao and D. Wang, *Nano. Lett.*, 2014, **14**, 6679.
16 Z. H. Yang, F. F. Xu, W. X. Zhang, Z. S. Mei, B. Pei and X. Zhu, *J. Power sources*, 2014, **246**, 24.
17 A. Indra, P. W. Menezes, C. Das, D. Schmeißer and M. Driess, *Chem. Commun.,* 2017, **53**, 8641.
18 F. Wang, W. Li, X. L. Feng, D. P. Liu and Y. Zhang, *Chem. Sci.,* 2016, **7**, 1867.
19 X. L. Guo, Z. H. Qiu, J. X. Mao and R. X. Zhou, *Phys. Chem. Chem. Phys.,* 2018, **20**, 25983.
20 Y. Hu, J. O. Jensen, W. Zhang, L. N. Cleemann, W. Xing, N. J. Bjerrum and Q. F. Li, *Angew. Chem. Int. Ed.*, 2014, **53**, 3675.
21 L. Cheng, Y. Men, J. G. Wang, H. Wang, W. An, Y. Q. Wang, Z. C. Duan and J. Liu, *Appl. Catal., B*, 2017, **204**, 374.
22 T. Y. Kou, C. H. Si, J. Pinto, C. Y. Mad and Z. H. Zhang, *Nanoscale,* 2017, **9**, 8007.
23 X. L. Guo, J. Li and R. X. Zhou, *Fuel*, 2016, **163**, 56.
24 A. B. Dongil, B. Bachiller-Baeza, E. Castillejos, N. Escalona, A. Guerrero-Ruiz and I. Rodríguez-Ramos, *Catal. Sci. Technol.,* 2016, **6**, 6118.
25 H. Wang, J. H. Shen, J. F. Huang, T. J. Xu, J. R. Zhu, Y. H. Zhu and C. Z. Li, *Nanoscale*, 2017, **9**, 16817.
26 Y. X. Gao, K. M. Xie, W. D. Wang, S. Y. Mi, N. Liu, G. Q. Pan and W. X. Huang, *Catal. Sci. Technol.,* 2015, **5**, 1568.
27 S. Q. Chen, L. P. Li, W. B. Hu, X. S. Huang, Q. Li, Y. S. Xu, Y. Zuo, and G. S. Li, *ACS Appl. Mater. Interfaces*, 2015, **7**, 22999.
28 T. E. James, S. L. Hemmingson, T. Ito and C. T. Campbell, *J. Phys. Chem. C*, 2015, **119**, 17209.
29 D. Jampaiah, S. J. Ippolito, Y. M. Sabri, B. M. Reddy and S. K. Bhargava, *Catal. Sci. Technol.,* 2015, **5**, 2913.
30 J. J. Sheng, C. T. Li, L. K. Zhao, X. Y. Du, L. Gao, G. M. Zeng, *Fuel*, 2017, **197**,397-406.
31 M. Konsolakisa and Z. Ioakeimidis, *Appl. Surf. Sci.,* 2014, **320**, 244.
32 N. Acerbi, S. C. Edman Tsang, G. Jones, S. Golunski and P. Collier, *Angew. Chem. Int. Ed.,* 2013, **52**, 7737.
33 T. R. Reina, S. Ivanova, O. H. Laguna, M. A. Centeno and J. A. Odriozola, *Appl. Catal., B*, 2016, **197**, 62.
34 A. Arango-Díaz, J. A. Cecilia, E. Moretti, A. Talon, P. Núñez, J. Marrero-Jerez, J. Jiménez-Jiménez, A. Jiménez-López and E. Rodríguez-Castellón, *Int. J. Hydrogen Energy*, 2014, **39**, 4102.

35 J. L. Ayastuy, E. Ferna´ndez-Puertas, M. P. Gonza´lez-Marcos and M. A. Gutie´rrez-Ortiz, *Int. J. Hydrog. Energy*, 2012, **37**, 7385.

36 X. L. Guo and R. X. Zhou, *J. Power Sources*, 2017, **361**, 39.

37 A. D. Benedetto, G. Landi and L. Lisi, *Catalysts,* 2018, **8**, 209.

38 W. W. Shen, D. S. Mao, Z. M. Luo and J. Yu, *RSC Adv.,* 2017, **7**, 27689.

39 W. W. Wang, P. P. Du, S. H. Zou, H. Y. He, R. X. Wang, Z. Jin, S. Shi, Y. Y. Huang, R. Si, Q. S. Song, C. J. Jia and C. H. Yan, *ACS Catal.*, 2015, **5**, 2088.

40 P. S. Barbato, S. Colussi, A. Di Benedetto, G. Landi, L. Lisi, J. Llorca, and A. Trovarelli, *J. Phys. Chem. C,* 2016, **120**, 13039.
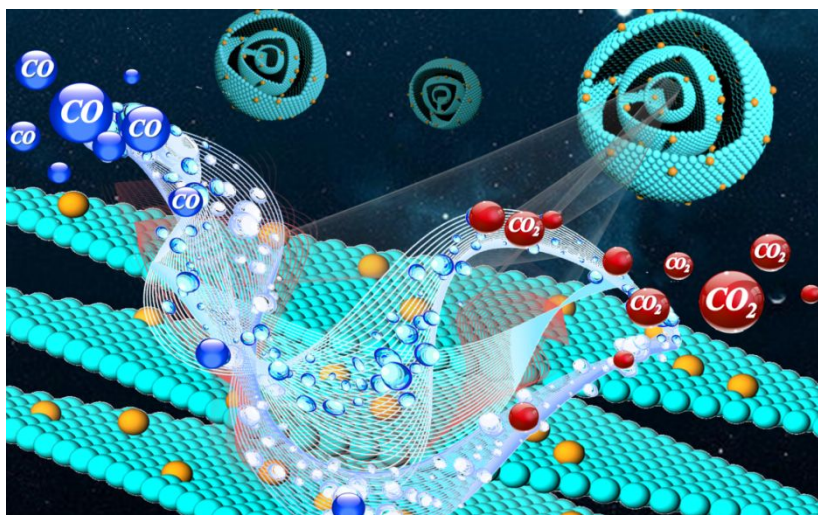
The triple-shelled CuO/CeO$_2$ exhibits superior catalytic performance for CO-PROX due to its fine-tunable geometric and electronic interactions.